

Symplectic Optimization on Gaussian States

Christopher Willby^{1,2}, Tomohiro Hashizume^{1,3}, Jason Crain^{4,2}, and Dieter Jaksch^{1,2,3}

¹*Institut für Quantenphysik, Universität Hamburg, 22761 Hamburg, Germany*

²*Clarendon Laboratory, University of Oxford, Parks Road, Oxford OX1 3PU, United Kingdom*

³*The Hamburg Centre for Ultrafast Imaging, Luruper Chaussee 149, D-22761 Hamburg, Germany and*

⁴*IBM Research Europe, The Hartree Centre STFC Laboratory, Sci-Tech Daresbury, Warrington WA4 4AD, UK*

Computing Gaussian ground states via variational optimization is challenging because the covariance matrices must satisfy the uncertainty principle, rendering constrained or Riemannian optimization costly, delicate, and thus difficult to scale, particularly in large and inhomogeneous systems. We introduce a symplectic optimization framework that addresses this challenge by parameterizing covariance matrices directly as positive-definite symplectic matrices using unit-triangular factorizations. This approach enforces all physical constraints exactly, yielding a globally unconstrained variational formulation of the bosonic ground-state problem. The unconstrained structure also naturally supports solution reuse across nearby Hamiltonians: warm-starting from previously optimized covariance matrices substantially reduces the number of optimization steps required for convergence in families of related configurations, as encountered in crystal lattices, molecular systems, and fluids. We demonstrate the method on weakly dipole-coupled lattices, recovering ground-state energies, covariance matrices, and spectral gaps accurately. The framework further provides a foundation for large-scale approximate treatments of weakly non-quadratic interactions and offers potential scaling advantages through tensor-network enhancements.

I. INTRODUCTION

Quadratic bosonic Hamiltonians form a fundamental class of models with Gaussian ground states [1–3]. These systems admit efficient phase-space representations, enabling the polynomial-time extraction of observables and correlation functions. Unlike fermionic systems, where diagonalization of the coupling matrix alone fully determines the ground-state properties [4, 5], the bosonic case is governed by an underlying symplectic phase-space structure imposed by the uncertainty principle. As a result, ground-state determination is equivalent to a symplectic diagonalization problem [1, 3, 6–8].

This additional structure introduces significant complexity and has hindered the development of a comprehensive, scalable numerical framework for obtaining ground-state properties of large bosonic quantum harmonic systems. In addition, the polynomial computational cost associated with symplectic diagonalization places severe practical limits on accessible system sizes. Nevertheless, the ability to compute ground states of large ensembles of quantum harmonic systems remains of practical and scientific interest, as such models underpin the established many-body dispersion method [9, 10], where access to larger system sizes is of particular importance for understanding the role of collective quantum effects in mesoscale processes, such as protein folding [11, 12].

Variational algorithms provide an alternative to exact diagonalization for solving many-body problems, often trading full spectral information for scalable, problem structure-exploiting optimization over a reduced variational manifold. In particular, optimization over the manifold of Gaussian states using Riemannian methods has been explored [13–17]. However, these approaches

face scalability challenges due to non-trivial constraint handling and the implementation of exponential maps. In particular, the retraction maps used in Ref. [13] and the quasi-geodesic approach of Ref. [15] require matrix exponentiation, leading to truncated power-series expansions and associated approximation errors. Additionally, the Cayley-transform-based methods employed in Refs. [14, 15] require matrix inversions at each gradient evaluation, which become computationally costly as the number of variational parameters increases.

Our key conceptual advance is a globally unconstrained symplectic parameterization of the Gaussian variational manifold. By constructing covariance matrices directly as positive-definite symplectic matrices via unit triangular factorization, the uncertainty principle is enforced exactly at every optimization step. This eliminates the need for penalty methods, or exponential maps, and converts the Gaussian ground-state problem into an unconstrained matrix trace minimization with exact symplectic structure preserved throughout.

Beyond single-instance optimization, solutions obtained for one Hamiltonian naturally act as effective preconditioners for nearby problems. Warm-starting the optimization from a ground-state covariance matrix at slightly modified couplings substantially reduces the number of optimization steps required. This stands in stark contrast to symplectic diagonalization, which does not permit such solution reuse. As a result, symplectic optimization is particularly well suited to settings involving large numbers of closely related configurations, such as density- or geometry-dependent scans in molecular fluids and complex chemical environments, where ground states must be recomputed repeatedly across similar instances [18].

We numerically validate our algorithm by solving

ground states of model quantum chemical systems consisting of ensembles of dipolar-interacting quantum Drude oscillators [10, 19, 20] on lattices, demonstrating clear accuracy for non-trivial chemical problems. While lattice implementations serve as convenient benchmarks, the framework itself is not restricted to lattice geometries and is directly applicable to describing quantum dipolar fluctuations in molecular fluids [21], where such effects are particularly important at complex interfaces [22, 23].

Our method for computing Gaussian ground states is based on iteratively evaluating traces of matrix-matrix products, leading to cubic scaling in the system size per evaluation. When only the spectral gap is required, this reduces to iteratively evaluating the trace of a congruence transformation involving a tall-skinny matrix whose row dimension is independent of the system size, making the procedure structurally analogous to Krylov-type estimators [24]. We observe empirical saturation for the quantum Drude lattice examples studied here, indicating empirically stable convergence behavior. Although the method remains subject to polynomial scaling due to its reliance on matrix multiplication, its practical efficiency arises from the fact that a fixed number of matrix contractions per step is required to construct Gaussian-state correlation matrices. This structure makes the algorithm structurally compatible with GPU acceleration [25].

More broadly, the value of this formulation lies in providing an unconstrained, reusable Gaussian optimization primitive that can be embedded within larger or more complex computational tasks. Accordingly, the method is not intended as a drop-in replacement for dense symplectic diagonalization in terms of wall-clock performance for single instance problems, but rather as a flexible variational component suited to iterative and composite problems, with the flexibility for future work to develop sparsity exploiting and tensor network algorithms for large and weakly non-quadratic bosonic systems.

II. SYMPLECTIC DIAGONALIZATION

Quadratic bosonic Hamiltonians, in the absence of linear terms, can be written compactly as

$$\hat{H} = \frac{1}{2} \hat{\mathbf{q}}^T H \hat{\mathbf{q}} \quad H > 0. \quad (1)$$

where H is the positive definite Hamiltonian matrix, where the positive definite constraint is written here as $H > 0 \leftrightarrow \mathbf{x}^T H \mathbf{x} > 0, \forall \mathbf{x} \in \mathbb{R}^d \setminus \{\mathbf{0}\}$ and $\hat{\mathbf{q}}^T = (\hat{x}_1, \dots, \hat{x}_d, \hat{P}_1, \dots, \hat{P}_d)$.

The $2d \times 2d$ matrix σ_{2d} , encodes the canonical commutation relations (CCR),

$$\sigma_{2d} = \begin{bmatrix} 0 & \mathbb{1}_d \\ -\mathbb{1}_d & 0 \end{bmatrix}, \quad (2)$$

where $[\hat{\mathbf{q}}_i, \hat{\mathbf{q}}_j] = i\sigma_{ij}$, setting $\hbar = 1$. A matrix which preserves the CCR and thus σ_{2d} under a transformation is a

symplectic matrix [3], belonging to the symplectic matrix group,

$$S\sigma_{2d}S^T = \sigma_{2d} \quad S \in \mathcal{S}_p(2d, \mathbb{R}). \quad (3)$$

This definition can also be generalized to rectangular symplectic matrices $\mathcal{S}_p(2k \times 2d, \mathbb{R})$, which are defined by $S\sigma_{2d}S^T = \sigma_{2k}$, $S \in \mathcal{S}_p(2k \times 2d, \mathbb{R})$, where σ_{2k} denotes the symplectic matrix given in Eq. (2) but restricted to a $2k$ -dimensional subspace i.e $\sigma_{2k} = \begin{bmatrix} 0 & \mathbb{1}_k \\ -\mathbb{1}_k & 0 \end{bmatrix}$, with $1 \leq k \leq d$. Henceforth, we write σ omitting the dimensional subscript.

Williamson's theorem [26] states there is always a $2d \times 2d$ symplectic matrix, which brings the positive definite matrix H into diagonal form, $SHS^T = \text{diag}(\epsilon_1, \epsilon_1, \dots, \epsilon_d, \epsilon_d)$, where ϵ_i are the symplectic eigenvalues of H , each repeated once along the diagonal. The set of symplectic eigenvalues or symplectic spectrum is unique for a given H [14, 27]. The ground state energy of \hat{H} is given by the sum of the symplectic eigenvalues [1, 3],

$$E_0 = \frac{1}{2} \sum_{i=1}^d \epsilon_i = \frac{1}{4} \text{tr}(SHS^T). \quad (4)$$

The energy gap, the energy deviation between the ground state and the first excited state, is given in terms of the symplectic eigenvalues as, $\Delta = \min_i \epsilon_i$. The vanishing energy gap, where $\Delta \rightarrow 0$, is called the critical limit. The symplectic eigenvalues and thus the ground-state energy are computable from the Hamiltonian matrix and σ as $\epsilon_i = \sqrt{\text{eig}_i(\sigma H \sigma^T H)}$ [1] or alternatively $\epsilon_i = \text{eig}_i(|\sigma H|)$ [28].

III. GAUSSIAN STATES

Gaussian states are the ground and thermal states of quadratic Hamiltonians in Eq. (1). The ground-state with density matrix $\hat{\rho}$, is completely characterized by its first moments, which are here set to zero without loss of generality, and a correlation matrix (CM) of two point correlation functions [1, 2]. The CM of correlation functions is given by the real, symmetric, $2d \times 2d$ matrix γ , an element of which is given in terms of the Gaussian density matrix as

$$\gamma_{ij} = \text{tr}[\hat{\rho} \{ \hat{\mathbf{q}}_i, \hat{\mathbf{q}}_j \}^+], \quad (5)$$

where $\{ \cdot, \cdot \}^+$ is the anti-commutator [1]. The uncertainty principle on the quadratures, can be written in matrix form, in the so-called Robertson-Schrödinger uncertainty relation, a multimodal matrix representation of the Heisenberg uncertainty principle,

$$\gamma + i\sigma \geq 0. \quad (6)$$

The constraint on the CM, given in Eq. (6) distinguishes it from the CM of a multivariate Gaussian probability distribution.

Using the definition of the variational principle expressed in terms of the density matrix and Eq. (5), we can formulate the variational problem for a quadratic bosonic Hamiltonian as follows [1]:

$$\begin{aligned} E_0 &= \inf_{\gamma} \frac{1}{4} \text{tr}(\gamma H) \quad \text{s.t.} \quad \gamma + i\sigma \geq 0, \\ \gamma_0 &= \arg \inf_{\gamma} \frac{1}{4} \text{tr}(\gamma H) \quad \text{s.t.} \quad \gamma + i\sigma \geq 0, \end{aligned} \quad (7)$$

where the constraint $\gamma + i\sigma \geq 0$ enforces the uncertainty principle, ensuring that the argument of Eq. (7) represents a valid CM.

IV. GAUSSIAN ANSATZ AND SYMPLECTIC OPTIMIZATION

The first result of this work builds on known parameterizations of Gaussian state CMs to establish a symplectic matrix parameterization, which is ideally suited for solving the variational problem in Eq. (7).

A real symmetric matrix is the CM of a pure Gaussian state of d modes, given by γ_p , iff it is both symplectic and positive definite (see Appendix A for proof),

$$\{\gamma_p\} = \mathcal{S}_p(2d, \mathbb{R}) \cap \mathbb{S}_{++}(2d, \mathbb{R}), \quad (8)$$

with $\{\gamma_p\}$ denoting the set of pure state CMs and we denote the set of real symmetric positive definite matrices of dimension $2d$, as $\mathbb{S}_{++}(2d, \mathbb{R})$. We thus construct an ansatz that explicitly encodes the space of admissible CM satisfying the uncertainty constraint. This ansatz serves as a symplectic parametrization of the feasible manifold over which the minimization in Eq. (7) is performed, as illustrated in Fig. 1 (a).

To make this parametrization operational, it is necessary to specify practical methods for generating symplectic positive definite matrices. In what follows, we present schemes based on matrix decompositions that ensure the symplectic constraint is exactly preserved. We employ factorizations in terms of unit triangular matrices, which provide a convenient and numerically stable way to parameterize elements of $\mathcal{S}_p(2d, \mathbb{R}) \cap \mathbb{S}_{++}(2d, \mathbb{R})$ [29, 30].

The elementary decomposition utilized here, are unit triangular matrices. A product of alternating unit triangular matrices is given as

$$\mathcal{L}_\nu = \begin{bmatrix} \mathbb{1}_d & M_1 \\ 0 & \mathbb{1}_d \end{bmatrix} \begin{bmatrix} \mathbb{1}_d & 0 \\ M_2 & \mathbb{1}_d \end{bmatrix} \cdots \begin{bmatrix} \mathbb{1}_d & 0 \\ M_{\nu-1} & \mathbb{1}_d \end{bmatrix} \begin{bmatrix} \mathbb{1}_d & M_\nu \\ 0 & \mathbb{1}_d \end{bmatrix} \quad (9)$$

with $M_i \in \mathbb{R}^{d \times d}$, $M_i^T = M_i$.

It has been shown in Ref. [30] that $\{\mathcal{L}_3^2\} = \mathcal{S}_p(2d, \mathbb{R}) \cap \mathbb{S}_{++}(2d, \mathbb{R})$, with $\mathcal{L}_\nu^2 = \mathcal{L}_\nu^T \mathcal{L}_\nu$. Given any symmetric matrix M_i can be freely parameterized in terms of $d \times d$ upper and lower triangular matrices, or the average of an arbitrary $d \times d$ matrix and its transpose, we can freely parameterize γ_p , through the product $\mathcal{L}_3^2 = \mathcal{L}_3^T \mathcal{L}_3$. This construction provides an explicit and *unconstrained* parametrization of the manifold of symplectic positive

definite matrices, ensuring that every choice of arbitrary matrix parameters yields a valid CM of a pure Gaussian state. Consequently, \mathcal{L}_3^2 serves as a convenient ansatz for generating admissible CMs that satisfy both the symplectic and positivity constraints required in Eq. (8). The \mathcal{L}_3^2 factorization uses three real symmetric $d \times d$ variable matrices M_1, M_2 , and M_3 to parametrize an arbitrary pure-state CM. This requires $3d(d+1)/2$ variational parameters, exceeding the $d(d+1)$ independent parameters of a pure Gaussian-state CM [3] by a factor of $3/2$. Whilst this overparametrization ensures that the full manifold of pure-state CMs is covered (with a non-unique parametrization), we find that it does not adversely affect convergence in the examples considered in this article.

Using the unconstrained parameterization of the Gaussian state CM, we rewrite the variational expression for the ground state energy in Eq. (7) as

$$\begin{aligned} E_0 &= \inf_{M_1, M_2, M_3} \frac{1}{4} \text{tr}(\mathcal{L}_3^T \mathcal{L}_3 H), \\ (M_1^0, M_2^0, M_3^0) &= \arg \inf_{M_1, M_2, M_3} \frac{1}{4} \text{tr}(\mathcal{L}_3^T \mathcal{L}_3 H). \end{aligned} \quad (10)$$

We have thus reformulated the Gaussian variational principle, as an unconstrained symplectic optimization (Sopt) problem, with cost function given by the trace of a series of matrix products. The corresponding ground state CM is then retrieved as, $\gamma_0 = (\mathcal{L}_3^0)^T \mathcal{L}_3^0$, where \mathcal{L}_3^0 is constructed from M_1^0, M_2^0 and M_3^0 , via Eq. (9). The cost-function, used for computing the Gaussian ground-state in Eq. (10), scales as $\mathcal{O}(d^3)$, per optimization step s , where s is defined as a call to the cost function. The dominant $\mathcal{O}(d^3)$ cost per step arises from the constant number of $2d \times 2d$ sized matrix multiplications, which scale cubically with the matrix dimension. Incorporating tensor network methods may further improve the scaling (see appendix B for details) [31].

In addition to ground state energy the Sopt framework can be used to compute the spectral gap. This is possible via unit triangular factorization, by projecting the symplectic CM into the appropriate sub-space, thereby maintaining the rectangular symplectic constraint. We define the projection matrix $P_1 = \begin{bmatrix} 1 & 0 & 0 & \cdots & 0 & 0 & 0 & \cdots & 0 \\ 0 & 0 & 0 & \cdots & 0 & 1 & 0 & \cdots & 0 \end{bmatrix} \in \mathbb{R}^{2 \times 2d}$, that selects the first position and first momentum component of $\mathcal{L}_3^T \mathcal{L}_3$, with $P_1 \mathcal{L}_3^T \in \mathcal{S}_p(2 \times 2d, \mathbb{R})$. Using the cyclicity of the trace and the symplectic trace minimization theorem (see Appendix C), this construction yields the variational estimate,

$$\Delta \leq \inf_{m_1, M_2, M_3} \frac{1}{4} \text{tr}(P_1 \mathcal{L}_3 H \mathcal{L}_3^T P_1^T), \quad (11)$$

which we empirically show is tight for the examples bench-marked here. While $M_1 \in \mathbb{R}^{d \times d}$ in the full parameterization, the action of P_1 leaves only a single row $m_1 = P_1 M_1 \in \mathbb{R}^d$ variational in Eq. (11); accordingly, the

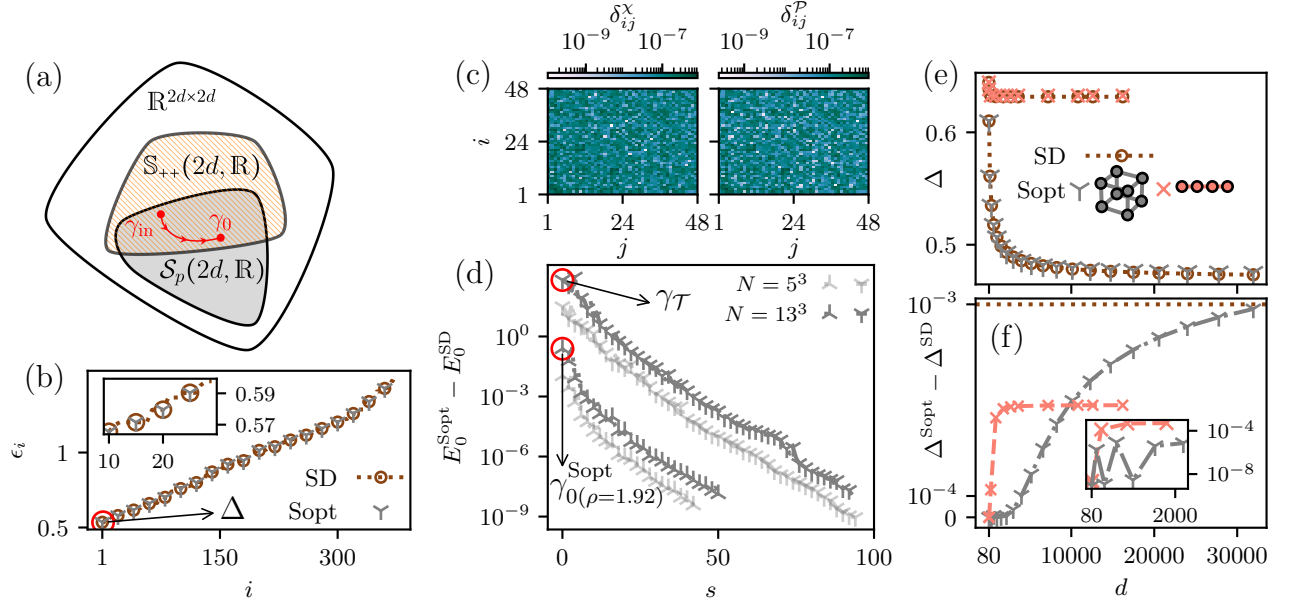


FIG. 1. (a) Schematic of the Gaussian variational manifold. The ground-state CM γ_0 lies in the intersection of the sets of symmetric positive-definite and symplectic matrices. The symplectic optimization (Sopt) procedure performs unconstrained optimization over this manifold using unit-triangular factorization, starting from an initial CM γ_{in} . (b-d) Validation of Gaussian ground-state recovery. (b) Agreement between the symplectic spectrum obtained via Sopt and that from symplectic diagonalization (SD) for a $d = 3(5 \times 5 \times 5)$ cubic lattice at $\rho = 1.9$. (c) Element-wise deviation between the CM retrieved via Sopt and that obtained from SD, shown for position correlations (left) and momentum correlations (right), displayed as log-scale heatmaps. (d) Convergence of the Sopt algorithm for cubic lattices of different sizes at $\rho = 1.9$, shown as the ground-state energy deviation $E_0^{\text{Sopt}} - E_0^{\text{SD}}$ versus the number of optimization steps s . Downward-pointing markers correspond to initialization from $\gamma_{\text{in}} = \gamma_{\mathcal{T}}$, while upward-pointing markers indicate a warm-started optimization initialized from the ground-state CM of the same lattice at $\rho = 1.92$. This preconditioning reduces the number of optimization steps required to reach a given accuracy by approximately a factor of two. (e-f) Energy gap Δ obtained via Sopt for cubic and chain lattices at $\rho = 2$ and $\rho = 1.9$, respectively, compared with SD. (f) Residual gap error after $s = 400$ optimization steps as a function of the number of lattice modes d . The inset highlights the low- d regime.

infimum is taken over (m_1, M_2, M_3) rather than over the full matrix M_1 .

Computing the cost function in Eq. (11), is dominated by multiplication between a tall-and-skinny matrix and a dense square matrix, owing to the dimensional reduction introduced by the projector P_1 . Consequently, the computational scaling per optimization step is $\mathcal{O}(d^2)$, which is a polynomial speedup, compared with Eq. (10).

V. NUMERICAL EXAMPLES

To demonstrate the capabilities of Sopt, for a model with a well studied solution, we consider assemblies of identically parametrized, dipole-coupled quantum Drude oscillators (QDOs) on lattices [32, 33]. We work in units of the identical oscillator frequency and thus the Hamiltonian matrix is $H = V \oplus \mathbb{1}_d$, where $V = \mathbb{1} + \rho^{-3}\mathcal{T}$ and \mathcal{T} is the dipole-dipole interaction matrix [34]. The dimensionless nearest-neighbor spacing ρ sets the interaction strength [32, 34]. Each QDO contributes three oscillator modes, so the total number of modes is $d = 3N$ for N

QDOs.

For block-diagonal quadratic Hamiltonians with no intermodal momentum couplings, such as the QDO Hamiltonian, the ground-state CM follows directly from diagonalizing V , yielding $\gamma_0 = V^{-1/2} \oplus V^{1/2}$ [1, 35, 36], with $V^{\pm 1/2} = O \text{diag}(\sqrt{\lambda_1^{\pm 1}}, \dots, \sqrt{\lambda_d^{\pm 1}}) O^T$, where O diagonalizes V and λ_i are its eigenvalues. For such structured Hamiltonians, the symplectic eigenvalues are given by $\epsilon_i = \sqrt{\lambda_i}$. We additionally benchmark the method on quadratic Hamiltonians with explicit position-momentum coupling, demonstrating comparable accuracy, reported in Appendix D.

For a proof-of-principle demonstration of Sopt, for solving QDO ensembles, we employ a conjugate-gradient (CG) method [37] (SciPy implementation) to solve the expression in Eq. (10), using the expressions for gradients of the variable matrices, given in the Appendix E, to construct the Jacobian. To further illustrate the straightforward trainability of the objective function, we also apply simple gradient-descent-based optimization schemes. Unless stated otherwise, we initialize the optimization with $M_1 = \rho^{-3}\mathcal{T}$ and $M_2 = M_3 = 0$, with resultant in-

tialization CM $\gamma_{\text{in}} = \gamma_{\mathcal{T}}$, where $\gamma_{\mathcal{T}} = \begin{bmatrix} \mathbb{1}_d + \rho^{-6}\mathcal{T}^2 & \rho^{-3}\mathcal{T} \\ \rho^{-3}\mathcal{T} & \mathbb{1}_d \end{bmatrix}$. This physically motivated choice significantly accelerates convergence, acting as an effective preconditioner. Although uninformed initializations converge to the same optimum, they typically require substantially more optimization steps to do so. This does not restrict generality, since an analogous initialization can always be constructed from the interaction matrix elements of a general quadratic Hamiltonian.

We refer to the ground-state CM, energy and gap computed via symplectic optimization as γ_0^{Sopt} , E_0^{Sopt} and Δ^{Sopt} , distinguishing them from the ground-state CM, energy and gap obtained via symplectic diagonalization (SD). All lattice calculations are preformed with open boundary conditions. For the $N = 3 \times 3 \times 3$ cubic lattice at $\rho = 1.9$, the Frobenius-norm error between γ_0^{Sopt} and γ_0^{SD} is 2.4×10^{-4} at CG solver tolerance 10^{-5} and 1.7×10^{-6} at tolerance 10^{-7} . At $\rho = 2.5$, the corresponding errors are 4.9×10^{-4} and 4.2×10^{-6} , respectively, indicating that the coupling strength does not significantly affect the accuracy. The unique symplectic spectrum of H is given by the eigenvalues of the optimized symplectic form of the Hamiltonian, $\mathcal{L}_3^0 H (\mathcal{L}_3^0)^T$, and is shown in Fig. 1(b) to overlap with the spectrum computed by SD at tolerance 10^{-5} , with a Frobenius-norm error between the two diagonal matrices of 3.0×10^{-5} . This demonstrates that γ_0^{Sopt} contains an accurate encoding of the symplectic spectrum of H . Fig. 1(c) shows the element-wise agreement between the position CM block given by $\delta_{ij}^X = |(\Pi_1^T \gamma_0^{\text{Sopt}} \Pi_1)_{ij} - (V^{-1/2})_{ij}|$ and for the momentum block $\delta_{ij}^P = |(\Pi_2^T \gamma_0^{\text{Sopt}} \Pi_2)_{ij} - (V^{1/2})_{ij}|$, where $\Pi_1^T = [\mathbb{1}_d, 0_d]$ and $\Pi_2^T = [0_d, \mathbb{1}_d]$, computed at tolerance 10^{-7} , and the ground-state CM obtained via diagonalization for a square lattice. The maximum errors in the two-point correlation functions are $\max(\delta_{ij}^X) = 8.4 \times 10^{-7}$ and $\max(\delta_{ij}^P) = 8.2 \times 10^{-7}$, both on the order of the solver tolerance.

In Fig. 1(d), we show the convergence of Sopt on cubic lattices of different sizes and with different initializations. Initializing the optimization with $\gamma_{\mathcal{T}}$, we find that the number of steps required to comparable accuracies given by $E_0^{\text{Sopt}} - E_0^{\text{SD}}$ increases only modestly as the cubic lattice size grows. After 30 steps, the error for the $N = 5 \times 5 \times 5$ cubic lattice is 1×10^{-3} , while for the order-of-magnitude larger $N = 13 \times 13 \times 13$ instance, a lower error of 9.8×10^{-4} is achieved after only 12 additional steps. Whilst not shown, we also consider $N = 10 \times 10$ and $N = 40 \times 40$ square lattices, where after 108 and 112 steps respectively the error in the ground-state energy is 2.1×10^{-9} and 6.6×10^{-8} . For both the square and cubic lattice, and for all considered sizes, 65 steps are sufficient to reduce the deviation from diagonalization below 10^{-4} . Fig. 1(d) further shows the convergence on the cubic lattice with a warm start. The initialization for the Sopt minimization is given by the ground-state CM of the same lattice setup at a 1% higher ρ value. This preconditioning reduces the number of steps required to

reach comparable accuracy to the $\gamma_{\mathcal{T}}$ initialization by approximately a factor of two, where 44 and 51 steps are required to reach accuracies of 1.4×10^{-8} and 2×10^{-9} for the $N = 5 \times 5 \times 5$ and $N = 13 \times 13 \times 13$ cases, respectively.

In Fig. 1 (e)–(f) we employ Sopt to determine the energy gap via Eq. (11). While the chosen symplectic parameterization ensures that the global minimum of the variational objective coincides with the exact ground-state energy, no analogous analytic guarantee exists for the extracting the spectral gap with unit triangular parametrization; nevertheless, we observe numerical convergence across all lattice sizes studied. We fix the number of optimization steps, $s = 400$, and consider a chain and cubic lattices. The Sopt algorithm is applied to determine the energy gap Δ in each case, using gradient descent with momentum (learning rate 0.26, momentum parameter 0.95). Fig. 1 (e), shows the convergent energy gap in the chain and the more gradually converging energy gap in the cubic lattice with increasing number of lattice modes. The lattice size dependent behavior in the energy gap is reflected in the convergence of Sopt, where the residual error, $\Delta^{\text{Sopt}} - \Delta^{\text{SD}}$, is shown in Fig. 1 (f). For the one-dimensional chain, we observe rapid saturation as a function of system size, with the error in the Sopt solution remaining constant to three decimal places at 5×10^{-4} , for $d \geq 900$. For the cubic lattice, the error increases beyond that of the chain, as a function of lattice size, however it remains below 1×10^{-3} at $d = 31,944$ modes.

VI. CONCLUSION

This work establishes a constraint-free reformulation of Gaussian ground-state optimization. In particular we have shown how the Gaussian variational problem can be recast as a symplectic optimization problem over the space of symplectic positive matrices. We then numerically demonstrated how to use symplectic optimization to find Gaussian ground states via unit triangular factorization of positive symplectic matrices. This results in a globally unconstrained symplectic trace minimization problem, which we carried out numerically for systems of dipole-coupled quantum Drudes on lattices.

Our symplectic optimization approach retrieves ground-state energies, correlation matrices, and spectral gaps in excellent agreement with symplectic diagonalization. While the benchmarks presented here correspond to quadratic Hamiltonians whose symplectic spectra are expressible as simple functions of the normal eigenvalues of the coupling matrix, the framework itself is fully general and directly applicable to non-block-diagonal quadratic Hamiltonians.

Whilst we have here focused on model quantum Drude systems, the methods can be straightforwardly be extended to realistic materials, within the many-body dispersion framework. It would be interesting to determine whether a practical computational advantage can

be achieved, owing to the reduced number of matrix multiplications required from reusing ground-states when cycling over a large number of closely related configurations. Such extensions could be of particular use, in exploring many-body quantum effects outside the realm of fixed lattice positions. For instance going beyond pairwise Stockmayer fluid descriptions [38, 39] via incorporating many-body quantum effects, across multiple configurations, would enable more accurate modeling of fluid-mediated self-assembly [40, 41].

Extensions of the method could explore approximating perturbative non-quadratic terms [42, 43] via symplectic optimization, utilizing the matrix parameterizations developed here. Such approaches could be useful for including higher-order multipole interactions between quantum Drudes at scale. A natural next step is to impose parameter reductions in the unit-triangular construction. Many physically relevant quadratic Hamiltonians are sparse, banded, or low-rank. Provided accuracy is retained under aggressive parameter reduction, dominant cost and gradient contractions could be reduced to sparse–sparse matrix multiplications. Such structure may also admit efficient tensor-network formulations and corresponding variational quantum algorithm implementations [44, 45], the full development of which we leave for future work. Finally, the proposed correlation-matrix parameterization may find applications in foundational studies, optimizing over the Gaussian-manifold, for problems with no known closed form solution [46–48].

ACKNOWLEDGEMENTS

Simulations were run on the University of Oxford Advanced Research Computing (ARC) facility. This work has received funding from the European Union’s Horizon Europe research and innovation program (HORIZON-CL4-2021DIGITAL-EMERGING-02-10) under grant agreement No. 101080085 QCFD. DJ and TH are partly funded by the Cluster of Excellence ‘Advanced Imaging of Matter’ of the Deutsche Forschungsgemeinschaft (DFG)—EXC 2056- project ID390715994. DJ acknowledges the support by DFG project “Quantencomputing mit neutralen Atomen” (JA 1793/1-1, JapanJST-DFG-ASPIRE 2024) and the Hamburg Quantum Computing Initiative (HQIC) project EFRE. The EFRE project is co-financed by ERDF of the European Union and by “Fonds of the Hamburg Ministry of Science, Research, Equalities and Districts (BWFGB)”.

Appendix A: Pure State CM Parameterization

The positivity constraint on the density matrix is enforced in phase-space by the Robertson-Schrödinger uncertainty relation on the CM. For a *pure* Gaussian state,

with CM given by γ_p , we have the following extra condition on the CM [49, 50],

$$\text{Det}(\gamma_p) = 1 \leftrightarrow (\gamma_p \sigma)^2 = -\mathbb{1}_{2d}. \quad (\text{A1})$$

This condition provides a general parameterization for pure state CMs:

Lemma 1. *A real symmetric matrix γ_p is the covariance matrix of a pure Gaussian state of d modes iff there exist real symmetric $d \times d$ matrices X and Y with $X > 0$ such that*

$$\gamma_p = \begin{bmatrix} X & XY \\ YX & YXY + X^{-1} \end{bmatrix}, \quad X > 0, Y = Y^T \& X = X^T. \quad (\text{A2})$$

See [49] for proof.

To prove the pure CM parameterization, utilized in the main-text, we make use of the following;

Lemma 2. *Any symmetric positive definite symplectic matrix can be written as*

$$\mathcal{S}_p(2d, \mathbb{R}) \cap \mathcal{S}_{++}(2d, \mathbb{R}) = \left\{ \begin{bmatrix} \mathbb{1}_d & 0 \\ Y & \mathbb{1}_d \end{bmatrix} \begin{bmatrix} X & 0 \\ 0 & X^{-1} \end{bmatrix} \begin{bmatrix} \mathbb{1}_d & Y \\ 0 & \mathbb{1}_d \end{bmatrix} \right\}, \quad (\text{A3})$$

where $\mathcal{S}_{++}(2d, \mathbb{R})$ denotes the set of matrices which are both positive definite and symmetric. Here X is symmetric ($X = X^T$) and positive definite ($X > 0$), and Y is symmetric.

See [51] for proof.

By expanding out the expression in Eq. (A3) and comparing to the parametrization for pure Gaussian state CMs in Eq. (A2), we prove the result stated in the main-text, that a symmetric positive definite symplectic matrix always constitutes a valid pure state CM.

Appendix B: Tensor Network Extension to the Method

In this appendix, we argue that the computational intractability of a large number of modes on current hardware can be addressed by decomposing the matrices M_ν and H into chains of tensors, called tensor networks (TN) [52–54], and optimizing individual tensors. To achieve this, we first discuss how a general $d \times d$ matrix \mathcal{M} is decomposed into contractions of tensors of rank 4, $\mathcal{T}_{\alpha_n, \alpha_{n+1}}^{\sigma_n, \sigma'_n}$. To this end, we find $\log_2 d$ tensors of the above form that give the element i, j of \mathcal{M} as

$$\mathcal{M}[i, j] = \sum_{\alpha_1, \alpha_2, \dots, \alpha_{\log_2 d-1}} \mathcal{T}_{\alpha_1, \alpha_2}^{\sigma_1, \sigma'_1} \dots \mathcal{T}_{\alpha_1, \alpha_3}^{\sigma_1, \sigma'_2} \mathcal{T}_{\alpha_n, \alpha_{n+1}}^{\sigma_n, \sigma'_n} \quad (\text{B1})$$

where σ_n and σ'_n correspond to the n^{th} bits of the binary representation of the indices i and j respectively ($i, j \in \{0, 1, \dots, \log_2 d - 1\}$). We see that the size of $\mathcal{T}_{\alpha_n, \alpha_{n+1}}^{\sigma_n, \sigma'_n}$ is at worst, $2 \times 2 \times \chi^2$, where the χ is the bond dimension (the largest range spanned by the bond indices

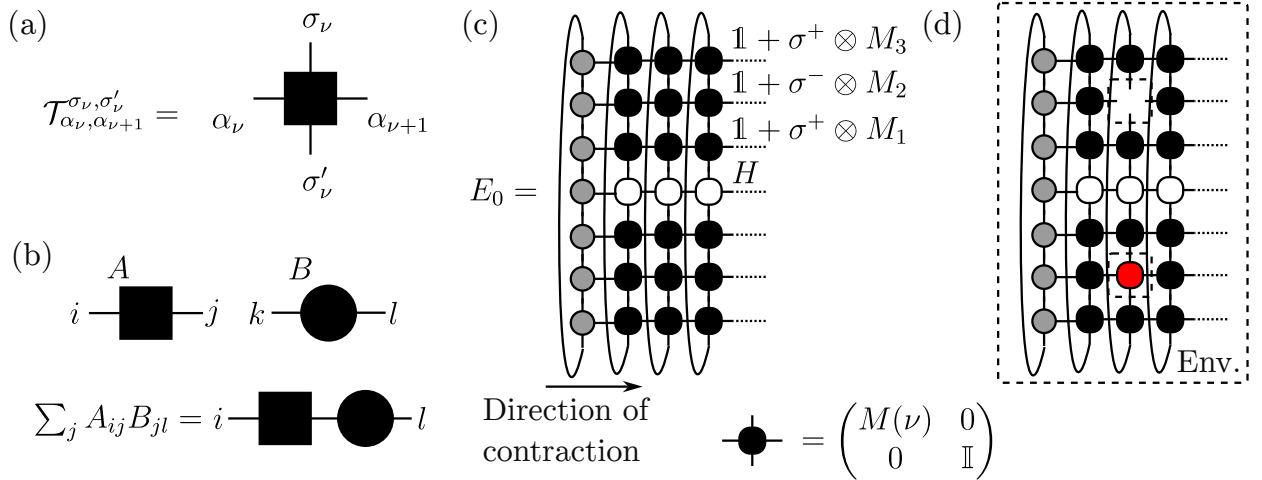


FIG. 2. (a) The graphical representation of a tensor $T_{\alpha_\nu, \alpha_{\nu+1}}^{\sigma_\nu, \sigma'_\nu}$. (b) The graphical representation of the product of two matrices A and B . The connection of two legs represents the contraction of shared matrix dimensions. (c) Tensor network diagram of the cost function E_0 . (d) networks required to compute the gradient of E_0 with respect to a local tensor, in this case, $M_2(2)$. The region wrapped by the dotted line containing two holes (one with a red tensor) is the environment of the local tensor $M_2(2)$. The full gradient is computed by summing term shown where the red tensor is replaced by $\begin{pmatrix} M_2(2) & 0 \\ 0 & 0 \end{pmatrix}$, the term where the red tensor is replaced by $\begin{pmatrix} 0 & 0 \\ 0 & \mathbb{I} \end{pmatrix}$, and their transposes. Here, \mathbb{I} is an identity matrix of the appropriate dimension and \mathbb{I} is the 2×2 identity matrix.

$\alpha_1, \dots, \alpha_{\log_2 - 1}$). By choosing a reasonable value for χ , the number of variational parameters to be optimized is reduced to $\mathcal{O}(\chi^2 \log_2 d)$, offering a potential exponential speed up for the ground state search.

To create \mathcal{L}_ν from Eq. (9) in the main text, we observe that (upper/lower) triangular matrices in the product are identical to $(\mathcal{I} + \sigma^{(+/-)} \otimes M_\mu)$, where

$$\sigma^+ = \begin{pmatrix} 0 & 1 \\ 0 & 0 \end{pmatrix}, \sigma^- = \begin{pmatrix} 0 & 0 \\ 1 & 0 \end{pmatrix}. \quad (\text{B2})$$

In terms of tensor networks, this is equivalent to prepending the tensor of bond dimension 1 that contains the appropriate σ^\pm , and placing the identity matrix in the lower right corner of each tensor after expanding the bond dimension of each tensor by 1.

In Fig. 2(a-d), we show the graphical notation for tensors and their contractions. In this notation, a tensor and its indices are denoted by a square and its legs, where the legs represent the indices. The contraction of two tensors is represented by two legs being connected (Fig. 2a). As an example, in Fig. 2b, we show the graphical representation of a product of two matrices. With this representation, the ground state energy, E_0 , (main-text Eq. (10)) can be represented as it is shown in Fig. 2c. The derivative of E_0 with respect to the ν^{th} local tensor $M_1(\nu) = T_{\alpha_\nu, \alpha_{\nu+1}}^{\sigma_\nu, \sigma'_\nu}$ of M_1 (similarly for M_2 and M_3) is, then, becomes a contraction of all the other local tensors except for $M(\nu)$ as shown in Fig. 2d.

Based on this, we find that the complexity for evaluating E_0 is $\mathcal{O}(\chi^7 \log_2 d)$. This optimal complexity is

achieved when the contraction is performed in the direction indicated by the arrows in Fig. 2c. Furthermore, to compute the derivative with respect to a local tensor, $\mathcal{O}(\chi^8)$ floating-point multiplications are required to create the environment (Fig. 2d, contracted network surrounded by the dotted line), and an additional $\mathcal{O}(\chi^4)$ is needed to compute the derivative.

In Fig. 3, we show the optimization results for quantum harmonic oscillators, restricted to fluctuate in one spatial dimension, residing on a cubic lattice of dimensions $d = 258 \times 258 \times 258$. We set the potential energies to unity and assigned a weight of 0.1 to the nearest-neighbor interactions. As shown, we found a configuration with an energy within $\approx 0.8\%$ of the exact energy, which is well below the trivial bound of $d/2$ (dashed line). The computation of 24×100 local optimization steps indicated by the star, took ≈ 15 hours on a single CPU (Intel(R) Xeon(R) CPU E5-2698 v4 @ 2.20GHz).

The true ground state energy is computed analytically by finding the exact expressions for the eigenvalues of the 256×256 matrix J , where the first off-diagonal elements are set to 0.1 to model a 1D nearest-neighbor chain. The k -th eigenvalue of J is expressed as $0.2 \cos \frac{k\pi}{\sqrt[3]{d+1}}$ [55]. Since the Hamiltonian is structured as a Kronecker sum of these matrices,

$$H = I + J \otimes I \otimes I + I \otimes J \otimes I + I \otimes I \otimes J \quad (\text{B3})$$

its eigenvalues are determined by all possible triplets of the eigenvalues of J . The final energy is obtained by summing the square roots of these combined eigenvalues across its entire spectrum.

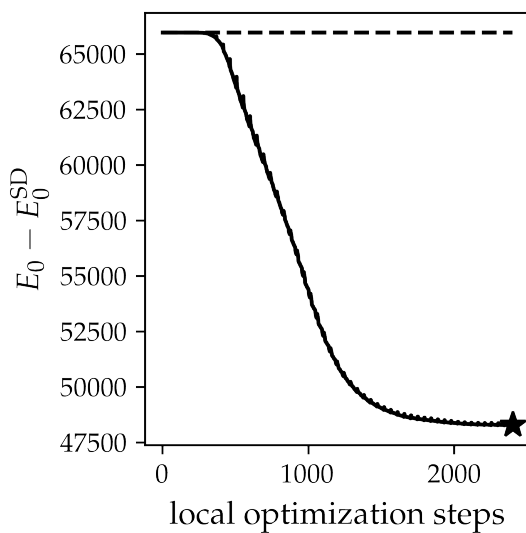


FIG. 3. The ground state energy of the bosons on a $d = 258 \times 258 \times 258$ cubic lattice, computed with the optimization of local tensors with $\chi = 4$ using the L-BFGS algorithm (10 modes, with 10 iterations) [56]. We set the potential energies to unity and assigned a weight of 0.1 to the nearest-neighbor interaction. The dashed line represents the trivial bound on the ground state energy, $d/2$. The optimization converged to within $\approx 0.8\%$ of the exact ground state energy $E_0^{\text{SD}} \approx 8.3226 \times 10^6$.

Appendix C: Symplectic Trace Minimization

A majorization relation among symplectic eigenvalues, proven by Hiroshima [57], allows the symplectic diagonalization problem to be reformulated as a symplectic trace minimization problem [14, 15]:

$$\inf_{X \in \mathcal{S}_p(2k \times 2d, \mathbb{R})} \frac{1}{4} \text{tr}(X H X^T) = \frac{1}{2} \sum_{i=1}^k \epsilon_i^\uparrow, \quad 1 \leq k \leq d. \quad (\text{C1})$$

Here ϵ_i^\uparrow denote the symplectic eigenvalues of H ordered increasingly. In the main text we demonstrated empirically that the choice $X = P_1 \mathcal{L}_3^T \in \mathcal{S}_p(2 \times 2d, \mathbb{R})$ accurately recovers the spectral gap via this variational principle.

More generally, we define the projector

$$P_k = \begin{bmatrix} \mathbb{1}_{k \times d} & 0_{k \times d} \\ 0_{k \times d} & \mathbb{1}_{k \times d} \end{bmatrix} \in \mathbb{R}^{2k \times 2d}, \quad (\text{C2})$$

where $\mathbb{1}_{k \times d}$ denotes the first k rows of a $d \times d$ identity matrix and $0_{k \times d}$ the corresponding rows of the zero matrix.

We extend the methods of the main text beyond the spectral gap and ground-state energy computation by considering the variational bound

$$\frac{1}{2} \sum_{i=1}^k \epsilon_i^\uparrow \leq \inf_{M_1, M_2, M_3} \frac{1}{4} \text{tr}(P_k \mathcal{L}_3 H \mathcal{L}_3^T P_k^T), \quad 1 \leq k \leq d. \quad (\text{C3})$$

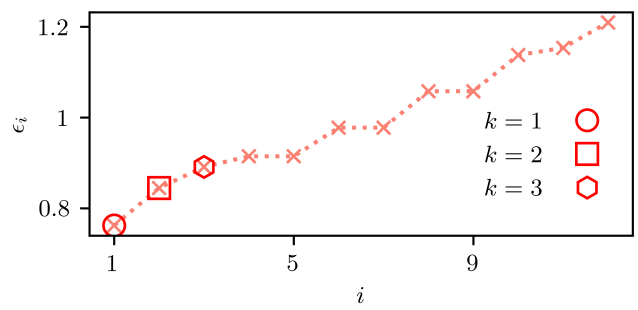


FIG. 4. Utilizing the majorization relation in Eq. (C1), we show here that Sopt can retrieve the first three symplectic eigenvalues of a 12 mode symplectic spectrum, where we numerically solve the optimization in Eq. (C3), for different k values.

To investigate the tightness of this bound, we consider the QDO system introduced in the main text, arranged on a 2×2 square lattice (a 12-mode system), with $\rho = 2$. We employ the conjugate gradient algorithm described previously to optimize the variational parameters in the matrices M_1 , M_2 , and M_3 . We note that this parametrization is already overparameterized for the spectral gap computation and is therefore likely overparameterized for the estimation of higher symplectic eigenvalue sums as well; nevertheless, it provides a flexible variational ansatz with which to assess the saturation of the bound in practice. Fig. 4 shows the agreement between the optimized symplectic spectrum and exact symplectic diagonalization for the first three symplectic eigenvalues, $\epsilon_1 \leq \epsilon_2 \leq \epsilon_3$, with the residual discrepancy set by the solver tolerance.

Appendix D: Non-Block Diagonal Hamiltonian

Here we extend the QDO model Hamiltonian considered in the main-text, to non-block diagonal couplings, with $2d \times 2d$ Hamiltonian matrix $H = \begin{pmatrix} V & c\mathbb{1}_d \\ c\mathbb{1}_d & \mathbb{1}_d \end{pmatrix}$, with the strength of the diagonal position—momentum coupling, given by $c \in \mathbb{R}$. In Fig. 5, we compare the ground-state energy computed via Sopt, with the ground-state energy computed via SD, using the same methods as outlined in the main-text. This shows the generalization of the Sopt framework to quadratic bosonic Hamiltonians with coupling between position and momentum operators.

Appendix E: Computing Gradients of Unit Triangular Cost Function

Here we derive expressions for the gradients, of the cost functions, in Eq. (9) and Eq. (11) given in the main-text.

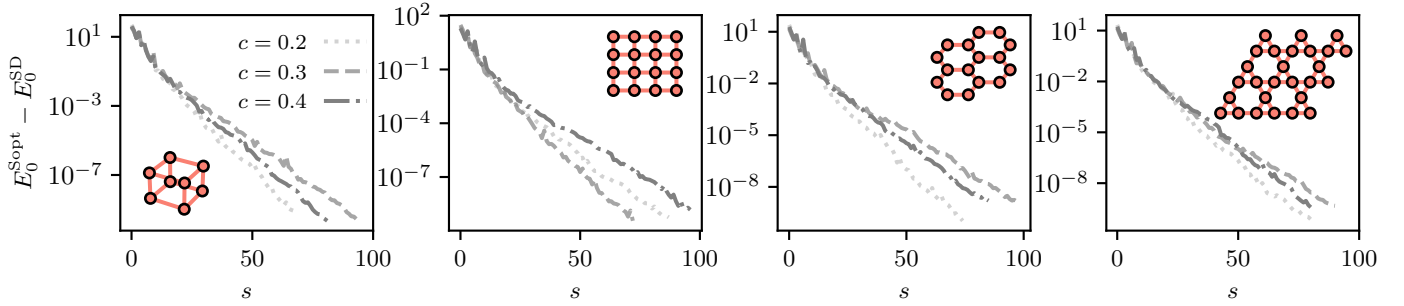


FIG. 5. Sopt accurately retrieves ground-state energies on dipole coupled lattices, amended with diagonal position momentum coupling, with coupling strength given by c . All lattice calculations are shown at $\rho = 1.9$, with $N = 5 \times 5 \times 5$ in (a), $N = 10 \times 10$ in (b), $N = 2 \times 7 \times 7$ in (c) and $N = 3 \times 5 \times 5$ in (d).

The gradient of $\frac{1}{4}\mathcal{L}_3 H \mathcal{L}_3^T$ with respect to \mathcal{L}_3 is [58],

$$\frac{1}{4} \nabla_{\mathcal{L}_3} \text{tr}(\mathcal{L}_3 H \mathcal{L}_3^T) = \frac{1}{2} \mathcal{L}_3 H \quad (\text{E1})$$

Then using chain rule and the cyclic property of the trace operator, one can derive general expressions for the gradients of the variable matrices M_1 , M_2 and M_3

$$\begin{aligned} \frac{1}{4} \nabla_{M_1} \text{tr}(\mathcal{L}_3 H \mathcal{L}_3^T) &= \Pi_1^T \mathcal{L}_3 H \Pi_2 M_3 M_2 + \Pi_1^T \mathcal{L}_3 H \Pi_2 \\ &\quad + \Pi_1^T \mathcal{L}_3 H \Pi_1 M_2, \end{aligned} \quad (\text{E2})$$

$$\begin{aligned} \frac{1}{4} \nabla_{M_2} \text{tr}(\mathcal{L}_3 H \mathcal{L}_3^T) &= M_1 \Pi_1^T \mathcal{L}_3 H \Pi_2 M_3 + M_1 \Pi_1^T \mathcal{L}_3 H \Pi_1 \\ &\quad + \Pi_2^T \mathcal{L}_3 H \Pi_2 M_3 + \Pi_2^T \mathcal{L}_3 H \Pi_1, \end{aligned} \quad (\text{E3})$$

$$\begin{aligned} \frac{1}{4} \nabla_{M_3} \text{tr}(\mathcal{L}_3 H \mathcal{L}_3) &= M_2 M_1 \Pi_1^T \mathcal{L}_3 H \Pi_2 + \Pi_1^T \mathcal{L}_3 H \Pi_2 \\ &\quad + M_2 \Pi_1^T \mathcal{L}_3 H \Pi_2. \end{aligned} \quad (\text{E4})$$

Here Π_1 and Π_2 are the basis matrices defined in the main-text.

For the block-diagonal Hamiltonian of the form $V \otimes \mathbb{1}_d$, we write out the gradient expressions, in terms of multiplications of $d \times d$ matrices, rather than the $2d \times 2d$ sized matrix multiplications. We use the explicit form of \mathcal{L}_3 ,

$$\begin{aligned} \mathcal{L}_3 &= \begin{bmatrix} \mathbb{1}_d & M_1 \\ 0 & \mathbb{1}_d \end{bmatrix} \begin{bmatrix} \mathbb{1}_d & 0 \\ M_2 & \mathbb{1}_d \end{bmatrix} \begin{bmatrix} \mathbb{1}_d & M_3 \\ 0 & \mathbb{1}_d \end{bmatrix} \\ &= \begin{bmatrix} \mathbb{1}_d + M_1 M_2 & M_3 + M_1 M_2 M_3 + M_1 \\ M_2 & M_2 M_3 + \mathbb{1}_d \end{bmatrix}. \end{aligned} \quad (\text{E5})$$

The gradients with respect to the variable matrices M_1 , M_2 and M_3 are given as,

$$\frac{1}{4} \nabla_{M_1} \text{tr}(\mathcal{L}_3 V \oplus \mathbb{1}_d \mathcal{L}_3^T) = (M_3 + M_1 M_2 M_3 + M_1)(\mathbb{1}_d + M_3 M_2) + (\mathbb{1}_d + M_1 M_2) V M_2 \quad (\text{E6})$$

$$\frac{1}{4} \nabla_{M_2} \text{tr}(\mathcal{L}_3 V \oplus \mathbb{1}_d \mathcal{L}_3^T) = M_1((M_3 + M_1 M_2 M_3 + M_1)M_3 + (\mathbb{1}_d + M_1 M_2)V) + (M_2 M_3 + \mathbb{1}_d)M_3 + M_2, \quad (\text{E7})$$

$$\frac{1}{4} \nabla_{M_3} \text{tr}(\mathcal{L}_3 V \oplus \mathbb{1}_d \mathcal{L}_3^T) = (\mathbb{1}_d + M_2 M_1)(M_3 + M_1 M_2 M_3 + M_1) + M_2(M_2 M_3 + \mathbb{1}_d). \quad (\text{E8})$$

We further include expressions for the gradient of Eq. (11) given in the main-text. We define $A = (B^T P_1)^T$ with $B = P_1 \mathcal{L}_3 H$. The definition of the projector $P_1 \in \mathbb{R}^{2 \times 2d}$, given in the main-text, selects the first position and momentum component of $\mathcal{L}_3^T \mathcal{L}_3$. Selecting differently

would require modification of the following gradient expressions. Defining the basis vectors $e_1^T = \underbrace{[1, \dots, 0, 0, \dots, 0]}_{2d}$ and $e_2^T = [0, \dots, 0, 1, \dots, 0]$, we have the following expres-

sions for the gradients of the variable vector m_1 and ma-

trices M_2 and M_3 ,

$$\nabla_{m_1} \frac{1}{4} \text{tr}(P_1 \mathcal{L}_3 H \mathcal{L}_3^T P_1) = e_1^T A \Pi_2 M_3 M_2 + e_1^T A \Pi_2 + e_1^T A \Pi_1 M_2, \quad (\text{E9})$$

$$\nabla_{M_2} \frac{1}{4} \text{tr}(P_1 \mathcal{L}_3 H \mathcal{L}_3^T P_1^T) = m_1 \otimes (e_1^T A \Pi_2 M_3 + e_1^T A \Pi_1) + \underbrace{(1, 0, \dots, 0)}_d \otimes (e_2^T A \Pi_1 + e_2^T A \Pi_2 M_3) \quad (\text{E10})$$

and

$$\nabla_{M_3} \frac{1}{4} \text{tr}(P_1 \mathcal{L}_3 H \mathcal{L}_3^T P_1) = M_2 m_1 \otimes e_1^T A \Pi_2 + \underbrace{(1, 0, \dots, 0)}_d M_2 \otimes e_2^T A \Pi_2 + \underbrace{(1, 0, \dots, 0)}_d \otimes e_1^T A \Pi_2. \quad (\text{E11})$$

Here \otimes denotes the outer product. Note that whether the number of variational parameters in Eq. (11) is optimal is not determined here, therefore the expressions in Eq. (E9) – Eq. (E11) may include redundant terms.

In the numerical implementation, the symmetric matrices M_k with $k \in \{1, 2, 3\}$ are parameterised via unconstrained upper-triangular matrices X_k as $M_k = \text{triu}(X_k) + \text{triu}(X_k)^T$. Gradients are therefore evaluated with respect to X_k and projected onto the symmetric subspace, which absorbs the factor 1/2 appearing in Eq. (E1).

REFERENCES

- [1] N. Schuch, J. I. Cirac, and M. M. Wolf, Communications in mathematical physics **267**, 65 (2006).
- [2] C. Weedbrook, S. Pirandola, R. García-Patrón, N. J. Cerf, T. C. Ralph, J. H. Shapiro, and S. Lloyd, Reviews of Modern Physics **84**, 621 (2012).
- [3] A. Serafini, *Quantum Continuous Variables: A Primer of Theoretical Methods* (CRC press, 2017).
- [4] J. Van Hemmen, Zeitschrift für Physik B Condensed Matter **38**, 271 (1980).
- [5] J. Colpa, Journal of Physics A: Mathematical and General **12**, 469 (1979).
- [6] O. Maldonado, Journal of Mathematical Physics **34**, 5016 (1993).
- [7] J. Colpa, Physica A: Statistical Mechanics and its Applications **93**, 327 (1978).
- [8] J. Colpa, Physica A: Statistical Mechanics and its Applications **134**, 377 (1986).
- [9] A. Tkatchenko, R. A. DiStasio Jr, R. Car, and M. Scheffler, Physical Review Letters **108**, 236402 (2012).
- [10] A. Khabibrakhmanov, D. V. Fedorov, A. Ambrosetti, J. Crain, K. L. Hunt, E. R. Johnson, K. D. Jordan, S. Góger, M. Gori, M. R. Karimpour, *et al.*, The Journal of Chemical Physics **163**, <https://doi.org/10.1063/5.0281913> (2025).
- [11] M. Stöhr and A. Tkatchenko, Science Advances **5**, eaax0024 (2019).
- [12] M. Gori, P. Kurian, and A. Tkatchenko, Nature Communications **14**, 8218 (2023).
- [13] B. Windt, A. Jahn, J. Eisert, and L. Hackl, SciPost Physics **10**, 066 (2021).
- [14] N. T. Son, P.-A. Absil, B. Gao, and T. Stykel, SIAM Journal on Matrix Analysis and Applications **42**, 1732 (2021).
- [15] B. Gao, N. T. Son, P.-A. Absil, and T. Stykel, SIAM Journal on Optimization **31**, 1546 (2021).
- [16] G. França, A. Barp, M. Girolami, and M. I. Jordan, arXiv preprint arXiv:2107.11231 <https://doi.org/10.48550/arXiv.2107.11231> (2021).
- [17] M. Gori, M. Sarkis, and A. Tkatchenko, Journal of Physics A: Mathematical and Theoretical **58**, 495304 (2025).
- [18] M. Reiher, N. Wiebe, K. M. Svore, D. Wecker, and M. Troyer, Proceedings of the national academy of sciences **114**, 7555 (2017).
- [19] F. Cipcigan, J. Crain, V. Sokhan, and G. J. Martyna, Reviews of Modern Physics **91**, 025003 (2019).
- [20] S. Góger, A. Khabibrakhmanov, O. Vaccarelli, D. V. Fedorov, and A. Tkatchenko, The Journal of Physical Chemistry Letters **14**, 6217 (2023).
- [21] A. Jones, F. Cipcigan, V. Sokhan, J. Crain, and G. Martyna, Physical Review Letters **110**, 227801 (2013).
- [22] F. S. Cipcigan, V. P. Sokhan, J. Crain, and G. J. Martyna, Journal of Computational Physics **326**, 222 (2016).
- [23] E. Feigl, M. Segal, and P. Jedlovszky, The Journal of Physical Chemistry B <https://doi.org/10.1021/acs.jpca.5c02397> (2025).
- [24] Y. Saad, *Numerical Methods for Large Eigenvalue Problems: Revised Edition* (SIAM, 2011).
- [25] M. S. Rudolph and J. Tindall, arXiv preprint arXiv:2507.11424 <https://doi.org/10.48550/arXiv.2507.11424> (2025).
- [26] J. Williamson, American Journal of Mathematics **58**, 141 (1936).
- [27] M. De Gosson, *Symplectic Geometry and Quantum Mechanics* (Springer, 2006).
- [28] S. Pirandola, A. Serafini, and S. Lloyd, Physical Review A **79**, 052327 (2009).
- [29] P. Jin, Y. Tang, and A. Zhu, SIAM Journal on Matrix Analysis and Applications **41**, 1630 (2020).

[30] P. Jin, Z. Lin, and B. Xiao, *Linear Algebra and its Applications* **650**, 236 (2022).

[31] N.-L. van Hülst, P. Siegl, P. Over, S. Ben-goechea, T. Hashizume, M. G. Cecile, T. Rung, and D. Jaksch, arXiv preprint arXiv:2507.05222 <https://doi.org/10.48550/arXiv.2507.05222> (2025).

[32] C. Willby, M. Kiffner, J. Tindall, J. Crain, and D. Jaksch, *Physical Review Letters* **135**, 110403 (2025).

[33] J. Cao and B. Berne, *The Journal of Chemical Physics* **97**, 8628 (1992).

[34] A. Donchev, *The Journal of Chemical Physics* **125**, 074713 (2006).

[35] K. Audenaert, J. Eisert, M. B. Plenio, and R. F. Werner, *Physical Review A* **66**, 042327 (2002).

[36] M. Cramer, J. Eisert, M. B. Plenio, and J. Dreissig, *Physical Review A* **73**, 012309 (2006).

[37] J. Nocedal and S. J. Wright, *Numerical Optimization* (Springer, 2006).

[38] B. Groh and S. Dietrich, *Physical Review E* **54**, 1687 (1996).

[39] S. Varghese, P. Illien, and B. Rotenberg, *The Journal of Chemical Physics* **163**, <https://doi.org/10.1063/5.0292306> (2025).

[40] T. Serwatka, R. G. Melko, A. Burkov, and P.-N. Roy, *Physical Review Letters* **130**, 026201 (2023).

[41] A. K. Singh, S. Puri, and V. Banerjee, *Physical Review E* **112**, 015420 (2025).

[42] T. Shi, E. Demler, and J. I. Cirac, *Annals of Physics* **390**, 245 (2018).

[43] T. Guaita, L. Hackl, T. Shi, C. Hubig, E. Demler, and J. I. Cirac, *Physical Review B* **100**, 094529 (2019).

[44] M. Lubasch, J. Joo, P. Moinier, M. Kiffner, and D. Jaksch, *Physical Review A* **101**, 010301 (2020).

[45] P. Siegl, G. S. Reese, T. Hashizume, N.-L. van Hülst, and D. Jaksch, *Physical Review Research* **8**, 013052 (2026).

[46] H. A. Camargo, L. Hackl, M. P. Heller, A. Jahn, T. Takayanagi, and B. Windt, *Physical Review Research* **3**, 013248 (2021).

[47] E. Aurell, L. Hackl, P. Horodecki, R. H. Jonsson, and M. Kieburg, *Physical Review Letters* **133**, 060202 (2024).

[48] M. Walschaers, *PRX quantum* **2**, 030204 (2021).

[49] M. M. Wolf, G. Giedke, O. Krüger, R. F. Werner, and J. I. Cirac, *Physical Review A* **69**, 052320 (2004).

[50] T. Hiroshima, G. Adesso, and F. Illuminati, *Physical Review Letters* **98**, 050503 (2007).

[51] F. M. Dopico and C. R. Johnson, *SIAM journal on matrix analysis and applications* **31**, 650 (2009).

[52] D. Perez-Garcia, F. Verstraete, M. M. Wolf, and J. I. Cirac, *Quantum Info. Comput.* **7**, 401–430 (2007).

[53] B. Pirvu, V. Murg, J. I. Cirac, and F. Verstraete, *New Journal of Physics* **12**, 025012 (2010).

[54] U. Schollwöck, *Annals of Physics* **326**, 96 (2011).

[55] W.-C. Yueh, *Applied Mathematics E-Notes* **5**, 66 (2005).

[56] C. Zhu, R. H. Byrd, P. Lu, and J. Nocedal, *ACM Transactions on Mathematical Software* **23**, 550 (1997).

[57] T. Hiroshima, *Physical Review A—Atomic, Molecular, and Optical Physics* **73**, 012330 (2006).

[58] K. B. Petersen, M. S. Pedersen, *et al.*, *Technical University of Denmark* **7**, 510 (2008).